Unconventional ideas for ionization cooling of muons

T.L. Hart,[a] J.G. Acosta,[a] L.M. Cremaldi,[a] D.V. Neuffer,[b] S.J. Oliveros,[a] D. Stratakis,[b] D.J. Summers[a,1] and K. Yonehara[b]

[a]*Department of Physics and Astronomy, University of Mississippi-Oxford,*
University, MS 38677, U.S.A.

[b]*Accelerator Division, Fermi National Accelerator Laboratory,*
Batavia, IL 60510, U.S.A.

E-mail: summers@phy.olemiss.edu

Abstract: Small muon beams increase the luminosity of a muon collider. Reducing the momentum and position spreads of muons reduces emittance and leads to small, cool beams. Ionization cooling has been observed at the Muon Ionization Cooling Experiment. 6D emittance reduction by a factor of $100,000$ has been achieved in simulation. Another factor of 5 in cooling would meet the basic requirements of a high luminosity muon collider. In this paper we compare, for the first time, the amount of RF needed in a cooling channel to previous linacs. We also outline three methods aimed to help achieve a final factor of 5 in 6D cooling.

---

[1]Corresponding author.

Contents

1 Introduction

Cool muons are needed for small beam sizes and high luminosity both for a Higgs Factory [1–3] and a high energy muon collider [4–6]. Small beam sizes also facilitate the acceleration of muons for a muon collider [7] or a neutrino factory [8, 9]. What principles can be used to rapidly create small beams? Muons passing through low Z absorbers lose both transverse and longitudinal momentum via ionization. RF cavities replace the lost longitudinal momentum. The result is transverse cooling from the lowered transverse momentum. Transverse cooling can be exchanged for longitudinal cooling if higher momentum muons pass through more material. The relations describing transverse ($\epsilon_\perp$ emittance) and longitudinal (ϵ_L emittance) cooling are given by [10, 11]:

$$\frac{d\epsilon_\perp}{ds} \simeq -\frac{g_t}{\beta^2}\frac{dE_\mu}{ds}\frac{\epsilon_\perp}{E_\mu} + \frac{1}{\beta^3}\frac{\beta_\perp^*}{2}\frac{(13.6\,\mathrm{MeV})^2}{E_\mu m_\mu c^2 L_R} \tag{1.1}$$

$$\frac{d\epsilon_L}{ds} \simeq -\frac{g_L}{\beta^2 E_\mu}\frac{dE_\mu}{ds}\epsilon_L + \frac{\gamma^3 \beta_L}{\beta c^2 p^2}\pi(r_e m_e c^2)^2 n_e(2-\beta^2) \tag{1.2}$$

where dE_μ/ds is the energy loss rate in the material. $\beta_\perp^*$ and β_L are transverse and longitudinal betatron functions which must be made small using strong magnetic and "RF/low momentum compaction" focusing, respectively. L_R is the absorber radiation length. $(L_R)(dE/ds)$ should be large to minimize multiple scattering per unit of absorbed energy. g_L and g_t are partition numbers that depend on beam dispersion and absorber geometry and permit transverse ($\epsilon_\perp$) to longitudinal (ϵ_L) emittance exchange.

$$g_{L,0} = -\frac{2}{\gamma^2} + \frac{2(\gamma^2 - \beta^2)}{\gamma^2 \left[\ln\left[\frac{2m_e c^2 \gamma^2 \beta^2}{I(Z)}\right] - \beta^2\right]} \tag{1.3}$$

$\epsilon_{\perp,\mathrm{eq}}$ and $\epsilon_{L,\mathrm{eq}}$ are the equilibrium emittances which are calculated as

$$\epsilon_{\perp,\mathrm{eq}} \simeq \frac{\beta_\perp^*(13.6\,\mathrm{MeV})^2}{2 g_t \beta m_\mu c^2 L_R\,(dE/ds)} \tag{1.4}$$

$$\epsilon_{L,\mathrm{eq}} \simeq \frac{\beta_L m_e c^2 \beta \gamma^2 (2 - \beta^2)}{4 g_L m_\mu c^2 \left[\ln\left[\frac{2m_e c^2 \gamma^2 \beta^2}{I(Z)}\right] - \beta^2\right]} \tag{1.5}$$

The longitudinal betatron function is given by

$$\beta_L = \sqrt{\frac{\lambda_{rf}\,\beta^3\,\gamma\,m_\mu c^2\,\alpha_p}{2\pi\,eV'\cos\phi_s}} \tag{1.6}$$

where V' is the average RF voltage gradient in a cell, λ_{rf} is the RF wavelength, and ϕ_s is the RF phase angle away from rising zero crossing. To first order α_p equals $1/\gamma^2$ for a linac with no dispersion, and $|1/\gamma^2 - 1/\gamma_t^2|$ for a lattice with dispersion such as a ring or a snake. By making the transition gamma close to the gamma of the beam, the momentum compaction, α_p, can be reduced. This decreases the longitudinal beta function and the longitudinal equilibrium emittance. Running near transition increases longitudinal momentum spread and reduces bunch length for a given longitudinal emittance. Reducing the RF wavelength does the same thing. Neither reduces the transverse partition number which would raise the transverse equilibrium emittance. The momentum spread is increased by reducing momentum compaction, which worsens chromaticity and possibly transmission.

1.1 Observation of ionization cooling at MICE

The first demonstration of ionization cooling by the Muon Ionization Cooling Experiment (MICE) shows that a long proposed method of shrinking a muon beam into a smaller volume works. MICE used superconducting focus coils surrounding a liquid hydrogen absorber encased by very thin aluminum windows to cool millions of large emittance muons. The magnets maximize the beam angular spread in the hydrogen. The angular divergence of a muon beam can be diminished until it reaches equilibrium with multiple Coulomb scattering in the material. So if there is more angular beam spread, there is more room to reduce and cool the beam spread. Ionization energy loss in MICE reduced transverse momentum. The MICE muon ionization cooling measurement is an important step towards a future muon collider, neutrino factory, and other cool muon experiments.

In detail, the international Muon Ionization Cooling Experiment (MICE [12–15]) at Rutherford Lab in the U.K. has measured transverse ionization cooling [16] by focusing muons with superconducting solenoids into liquid hydrogen [17, 18] and lithium hydride energy absorbers. The technique measures an increase in the core density of an ensemble of muons constructed from individual muons [19–21]. Measurements to improve understanding of muon multiple scattering have been performed both at MICE [22] and at TRIUMF [23]. Data with muons passing through a polyethylene wedge [24–26] have been recorded to allow measurement of longitudinal to transverse emittance exchange in both directions [27]. MICE has a well characterized muon beam [28–30].

In summary, MICE has used 140 MeV/c muons with normalized transverse emittances of 6 mm and 10 mm. A reduction in the transverse amplitude of muons, when they pass through liquid hydrogen and lithium hydride absorbers, is observed. No reduction is seen when the absorbers are removed. The probability that this effect is a fluctuation is less than 10^{-5}. Monte Carlo simulations show the same reductions [31].

2 Helical cooling channel

The helical cooling channel has the advantage of using hydrogen which has less multiple scattering than lithium hydride. However, the continuous solenoidal field limits the strength of focusing, i.e., $1/\beta^*$. Recently the momentum compaction of the channel has been lowered by using additional coils. This has reduced the longitudinal emittance from 1540 microns [32] to 890 microns [33]. The hydrogen in the channel neutralizes space charge and permits short bunch lengths [34–36]. Operating RF cavities in magnetic fields can lead to breakdown [37, 38]. However, tests show that pressurized hydrogen gas can prevent breakdown in RF cavities in ionizing beams and magnetic fields [39]. Muon transport in plasma is under study [40]. Using beryllium for RF cavities also ameliorates breakdown in a magnetic field [41].

3 Rectilinear cooling channel

The rectilinear ionization cooling channel [42, 43] is a tightly spaced lattice containing wedge absorbers for reducing the x, y, and z momentum of the muon beam, RF cavities for restoring longitudinal muon momentum, and solenoids for focusing the beam. The net loss in transverse momentum results in cooling. Tilted solenoids create dispersion and spread the muons in the wedges as a function of momentum. Higher momentum muons lose more energy. As a result, emittance is periodically exchanged between the longitudinal and transverse degrees of freedom, resulting in cooling in all three phase space planes.

The rectilinear cooling channel has 12 linear stages. Cells from stages B1 and B8 are shown in figure 1. Stages are constructed with short superconducting solenoids up to 14 T for focusing, energy absorbers such as lithium hydride wedges to actually cool muons by removing transverse momentum, and 325 and 650 MHz normal conducting RF cavities to reaccelerate muons longitudinally. As one moves along the channel, each stage has a smaller minimum betatron function to increase cooling and lower emittance. Larger maximum betatron functions in successive stages can be tolerated if muons are cooler. Note that $\beta_{\max} = L^2/\beta_{\min}$, where L is the distance between the focusing magnets and the absorber [44].

The rectilinear channel [42] is tapered (also true of the helical channel) and grows smaller transversely as the muon beam cools [45]. Short solenoids provide strong focusing in short regions. The solenoids achieve a β^* of 3 cm in a lithium hydride absorber in the twelfth and final stage. In simulation, the channel works both with vacuum and with hydrogen to prevent breakdown in the RF cavities [46].
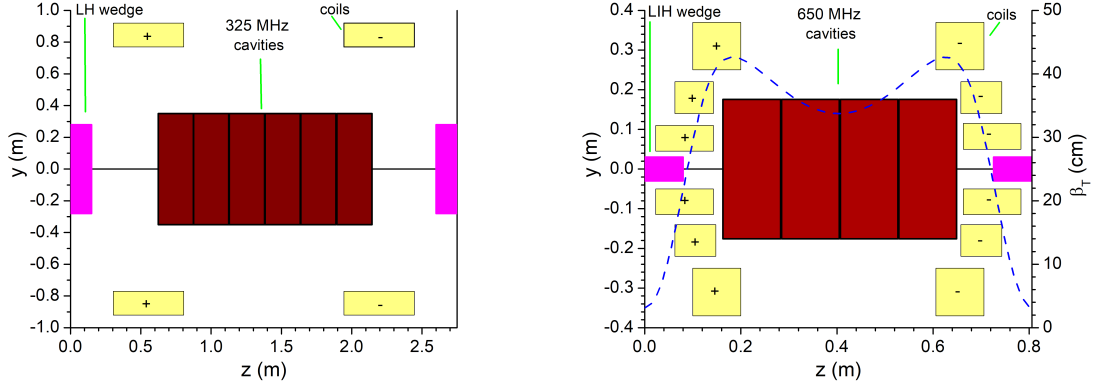

Figure 1. One cell of stage B1 in the middle of the Rectilinear Cooling Channel [42] is shown on the left. B1 follows stages A1, A2, A3, and A4. One cell of stage B8 (right) is at the end of rectilinear cooling.

3.1 Rectilinear and helical cooling channel comparison

Helical [32, 33] and rectilinear [42] cooling channels have been simulated as noted in table 1. They come close to achieving the cooling desired for a muon collider. The helical channel is based on a gradually tapered solenoidal magnetic field with high pressure hydrogen as a continuous absorber. It achieves a normalized longitudinal emittance of 890 microns [33], better than the 1570 microns of the rectilinear channel. Lower longitudinal emittance may also be possible in the rectilinear channel. The rectilinear channel uses a varying solenoidal magnetic field with lithium hydride wedges placed in short, low betatron regions for final cooling. It achieves a normalized transverse emittance of 280 microns [42]. Noting from eq. (1.4) that $\epsilon_{\perp,\text{eq}} \propto \beta_{\perp}^* / L_R (dE/ds)$ we find that [10]

$$\frac{\epsilon_{\perp,\text{eq}}(\text{helical})}{\epsilon_{\perp,\text{eq}}(\text{rectilinear})} = \frac{9.5\,\text{cm}}{252.6\,\text{MeV}} \times \frac{152\,\text{MeV}}{3.0\,\text{cm}} = 1.9 \tag{3.1}$$

The helical channel has less multiple scattering because it uses hydrogen while the rectilinear channel has a lower $\beta_{\perp}^*$. A 14 T solenoidal magnetic field gives $\beta_{\perp}^*$ of 9.5 cm [47]. Overall one expects a 1.9× lower transverse emittance from the rectilinear channel. This can also be seen in table 1. The helical and rectilinear channels achieve factors of 40, 000 and 108, 000 in 6D cooling, respectively. Cooling by a factor of 500, 000 is needed for a 10^{34} cm^{-2} s^{-1} high energy muon collider. Possible methods to get the factor of 5 improvement are described in this paper. The 20% rectilinear channel transmission noted in table 2 can deliver the 2×10^{12} μ^+ and μ^- bunches needed for the 10^{34} cm^{-2} s^{-1} collider. There is a factor of 1.5 margin in muon production to allow for losses in additional cooling and in acceleration.

Table 1. Simulated Helical and Rectilinear Cooling Channel normalized 6D emittances plus the emittance desired for a high energy muon collider in the last line. The initial 21 bunches are merged during cooling [48].

	ϵ_x (mm)	ϵ_y (mm)	ϵ_z (mm)	ϵ_{6D} (mm^3)
Initial Emittance [42]	17.0	17.0	46.0	13,300
Helical Cooling 1 [32]	0.523	0.523	1.54	0.421
Helical Cooling 2 [33]	0.61	0.61	0.89	0.331
Rectlinear Cooling [42]	0.28	0.28	1.57	0.123
Muon Collider [49]	0.025	0.025	72	0.045

3.2 Cooling both positive and negative muons in one rectilinear channel

One 12 stage rectilinear channel (see table 2) may be able to cool both muon signs, saving a factor of two in cost. In each stage, μ^+ and μ^- beams would go in opposite directions, before proceeding to the next stage. Each stage would require an exit kicker on each end for a total of 24 kickers. The stage A1 exit has the largest normalized transverse emittance, 6.28 mm. The head of a 65 ns long bunch train takes 440 ns to travel through the 132 m A1 channel. A kicker would need to rise in 375 ns (440–65). A ring kicker designed for a normalized transverse emittance of 10 mm, a rise time of 50 ns, and a 30 m circumference muon cooling ring required 5700 kV with one loop [50]. The voltage is high. Even splitting circuits may not help enough. The voltage for this exit kicker may be low enough to work:

$$V_{1\,\text{loop}} = (5700\,\text{kV})(6.28\,\text{mm}/10\,\text{mm})(50\,\text{ns}/375\,\text{ns}) = 480\,\text{kV} \tag{3.2}$$

3.3 Feasibility of the rectilinear RF system

We next calculate the peak and average RF power of the rectilinear cooling channel. Then we compare these two values to previous linacs to gauge affordability. The energy stored per meter in a pillbox RF cavity is given by

$$U = \frac{\epsilon}{2} E_0^2 \, (J_1(2.405))^2 \, \pi R_c^2 = \frac{\epsilon}{2} E_0^2 \, (0.519)^2 \, \pi \left(\frac{2.405\,c}{2\pi f} \right)^2 = 49400 \left(\frac{E_0}{f} \right)^2 \text{joules/m} \tag{3.3}$$

where $\epsilon = 8.85 \times 10^{-12}$ Farads/m (the permittivity of free space), J_1 is a Bessel function, and c is the speed of light. Equation (3.3) is used to calculate the 'RF total [Joules]' column in table 2.

Next calculate the filling time (τ), duty factor (DF) with an 0.5 µs flat top, peak power (P), and average power for the 325 MHz RF cavities [51], (see table 3):

$$\tau = \frac{Q}{\omega} = \frac{25000}{2\pi \times 325 \times 10^6} = 12.2\,\mu\text{s} \tag{3.4}$$

$$\text{Pulse Length} = ((3 \times \tau) + 0.5)\,\mu\text{s} = 37.2\,\mu\text{s}$$

$$\text{DF} = 37.2\,\mu\text{s} \times 15\,\text{Hz} = 5.6 \times 10^{-4}$$

$$P = \omega \frac{U}{Q} = 2\pi \times 325 \times 10^6 \frac{83420}{25000} = 6814\,\text{MW}$$

$$P_{\text{AVG}} = 6814\,\text{MW} \times 5.6 \times 10^{-4} = 3.8\,\text{MW}$$

Now repeat the calculation for the 650 MHz RF cavities:

$$\tau = \frac{Q}{\omega} = \frac{20000}{2\pi \times 650 \times 10^6} = 4.90\,\mu s \tag{3.5}$$

$$\text{Pulse Length} = ((3 \times \tau) + 0.5)\,\mu s = 15.2\,\mu s$$

$$\text{DF} = 15.2\,\mu s \times 15\,\text{Hz} = 2.3 \times 10^{-4}$$

$$P = \omega \frac{U}{Q} = 2\pi \times 650 \times 10^6 \frac{22450}{20000} = 4584\,\text{MW}$$

$$P_{\text{AVG}} = 4584\,\text{MW} \times 2.3 \times 10^{-4} = 1.1\,\text{MW}$$

SLAC was powered by 245 65 MW klystrons, which provided a peak power of 15925 MW to the SLED system, which compressed RF pulses. Because of efficiency, AC wall power is roughly twice the average power. From table 3, the ratio of peak power for muon cooling to that at SLAC is (6814 + 4584) / 15925 = 0.72. The average RF power for cooling muons is less than that in accelerators at SLAC, LEP, and LAMPF. RF systems as large as that required for muon cooling have been previously built. Higher frequency RF may be possible in the later stages of the rectilinear channel to lower power consumption and to lower longitudinal emittance.

Table 2. Rectilinear RF parameters [42]. The RF phase is the angle away from rising zero crossing.

Stage (Cells)	Cell length [m]	Total length [m]	RF freq [MHz]	RF gradient [MV/m]	RF # per cell	RF length [cm]	RF total length [m]	RF total [GV]	RF total [Joules]	RF phase [deg]	Muon Transmission [%]
A1 (66)	2.000	132.00	325	22.0	6	25.50	100.98	2.22	22900	14	70.6
A2 (130)	1.320	171.60	325	22.0	4	25.00	130.00	2.85	29400	15	87.5
A3 (107)	1.000	107.00	650	28.0	5	13.49	72.17	2.02	6620	20	88.8
A4 (88)	0.800	70.40	650	28.0	4	13.49	47.48	1.33	4350	16	94.6
B1 (20)	2.750	55.00	325	19.0	6	25.00	30.00	0.57	5070	41	89.7
B2 (32)	2.000	64.00	325	19.5	5	24.00	38.40	0.75	6830	41	90.6
B3 (54)	1.500	81.00	325	21.0	4	24.00	51.84	1.09	10700	39	89.2
B4 (50)	1.270	63.50	325	22.5	3	24.00	36.00	0.81	8520	49	89.7
B5 (91)	0.806	73.35	650	27.0	4	12.00	43.68	1.18	3720	49	87.5
B6 (77)	0.806	62.06	650	28.5	4	12.00	36.96	1.05	3510	49	88.0
B7 (50)	0.806	40.30	650	26.0	4	12.00	24.00	0.62	1900	46	89.6
B8 (61)	0.806	49.16	650	28.0	4	10.50	25.62	0.72	2350	47	89.0
325 Total		567.10			1562		386.77	8.29	83420		
650 Total		402.27			2003		249.91	6.92	22450		
Total		969.37			3565		636.68	15.22	105870		20.7

Table 3. RF power comparison.

Machine	Frequency [MHz]	No. of RF cavities	RF length [m]	No. of Kly-strons	Klystron peak [MW]	Peak power [MW]	Pulse Length [μs]	Rep Rate [Hz]	Average Power [MW]
Rectilinear [42]	325	1562	387	TBD	TBD	6814	37.2	15	3.8
Rectilinear	650	2003	250	TBD	TBD	4584	15.2	15	1.1
SLAC [52, 53]	2856	75000	2926	245	65	15925	3.5	120	6.7
LEP [54]	352	1376	585	40	0.6	24	CW	CW	24.0
LAMPF [55]	201.25			4	2.5	10	1000	120	1.2
LAMPF	805			44	1.2	52.8	1000	120	6.3

4 Quadrupole cooling channel

Low equilibrium emittance requires low $< \beta_\perp >$. Strong quadrupole focusing [56–58] can achieve $\beta_\perp^*$ values below the 3 cm achieved in the final stage of the rectilinear cooling channel design, (see figure 2 and table 4). A low p_z spread is used to control chromaticity in the channel. The input longitudinal emittance is reduced to 632 microns to achieve the low p_z spread. The longitudinal emittance is reduced by lowering β_L, which is defined by eq. (1.6). The 1300 MHz RF frequency helps to do this, as well as the high RF real estate fraction of 52%. There is 0.75 m of RF in a 1.44 m cell.

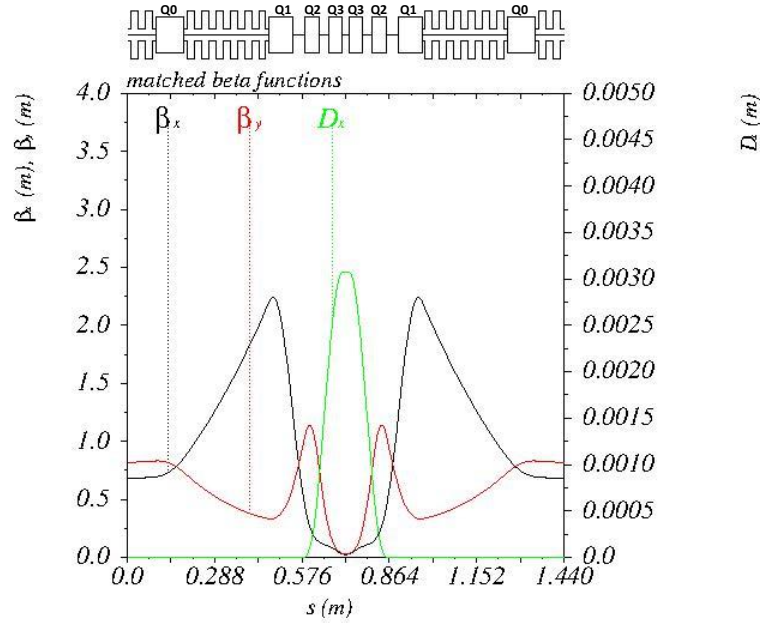Reducing beam momentum decreases muon straggling which is good, but also dictates shorter,

Figure 2. Full cell betatron function vs. distance s. The Courant-Snyder [67] parameter evolution through the cell are given by MAD-X [65, 66]. The betatron function values are $(\beta_x^*, \beta_y^*) = (2.2, 2.7)$ cm in the middle and $(\beta_x, \beta_y) = (0.681, 0.820)$ m at the ends.

Table 4. Superconduction quadrupole parameters.

	Bore Diameter	Bore Length	Gap to Next Quad	Pole Tip Field
Q0	10.0 cm	9.375 cm	28.125 cm	0.962 T
Q1	11.0 cm	7.875 cm	3.175 cm	6.82 T
Q2	5.3804 cm	4.875 cm	3.0 cm	9.96 T
Q3	3.94832 cm	4.5 cm	2.25 cm	10.0 T

more difficult to build, quadrupoles. A half cell is composed of four quadrupole magnets; the magnet Q0 is a coupling quadrupole preceded by two RF (radio frequency) cavities (L = 0.046875 m) and separated from Q1 by six RF (L = 0.046875 m) cavities. The RF cavities have a radius of 0.125 m. The 1300 MHz RF has a phase angle 11.5° away from rising zero crossing and a 27.8722 MV/m gradient.

The quadrupoles are short and close together. Fringe fields are an issue [59]. The quadrupole fields will need to be a maximum at the center and then fall [60]. For parameters of the quadrupoles, which use either NbTi or Nb$_3$Sn conductor, see table 4. The Q0 magnet works as a coupling quadrupole reducing the betatron function maximum and allows the addition of more RF cavities to increase longitudinal synchrotron focusing. The quadrupole Q3 is added to reduce both the chromaticity and the minimum beta function. The 144 cm long full cell has a 2.25 cm drift space for an absorber. The quadrupoles Q2 and Q3 have a dipole magnetic component to produce a uniform dispersion of 2.900 mm at the absorber space [61–64]. The betatron function evolution for the full cell is shown in figure 2. The transported beam has $\beta_{x,max} \cong 2\beta_{y,max}$.

4.1 Full cell constraints

MAD-X [65, 66] is used to set magnet parameters to constrain the beta functions and dispersion at the center of the absorber. Dispersion is flat and constant at the absorber locations and zero at the cell ends. The average transverse betatron function over the 2.25 cm long absorber area is less than 3.0 cm for a 300 MeV/c muon. The quadrupole doublet configuration is designed for a beam near 300 MeV/c. (β_x^*, β_y^*) equals (2.2, 2.7) cm at the centers of the absorbers.

As shown in figure 2, β^* is small only over a limited longitudinal distance, so the absorber must be dense and short [11]. For this configuration, the absorber is 2.25 cm long at the reference orbit, which is a good match to β_x^* and β_y^*.

4.2 Wedge for emittance exchange

The Q2, Q3 quadrupoles have dipole magnetic field components of 0.667 T and 0.475 T calculated to create a constant $\eta = 2.9$ mm dispersion at the absorber region as figure 2 shows.

A 40° lithium hydride wedge is placed at the center of the 1.44 m long full cell. The ends of the wedge extend into the Q3 magnet bores on each side of the wedge. The wedge geometry and the dispersion magnitude modify the partition numbers [10] as follows:

$$g_L = g_{L,0} + \frac{\eta}{W}, \, g_x = 1 - \frac{\eta}{W} \tag{4.1}$$

where η is the dispersion magnitude, and W is the distance from the wedge apex to the orbit reference center. The natural longitudinal partition number, $g_{L,0}$, is -0.063; this must be adjusted by emittance exchange between the (x, z) directions through wedge absorbers placed in dispersive regions. The values for η and W, 2.9 mm and 30.909 mm, respectively, are chosen to reduce the equilibrium longitudinal emittance at the expense of the equilibrium x emittance. This emittance exchange prevents severe longitudinal beam heating and results in the normalized longitudinal emittance remaining constant, and transverse beam cooling. Consecutive cells have opposite bending directions to make a snake channel configuration.

4.3 First stage simulation

When the absorbers and RF are included and the stochastic processes are enabled, the transmission drops to 7600/10000 initial muons. Figure 3 shows transmission vs. distance. Higher transmission would be better. Assume that four stages will be needed. 0.76^4 equals 0.33, but 0.90^4 equals 0.65. Therefore, 90% transmission requires half as many protons to generate muons as 76% transmission.

The first channel stage was simulated using ICOOL [68, 69] and had initial emittances of $\epsilon_{x,y,z} = (0.330, 0.246, 0.632)$ mm with the three normalized emittances uncorrelated. If proper beam correlations are introduced, transmission improves. Higher momentum muons need to follow
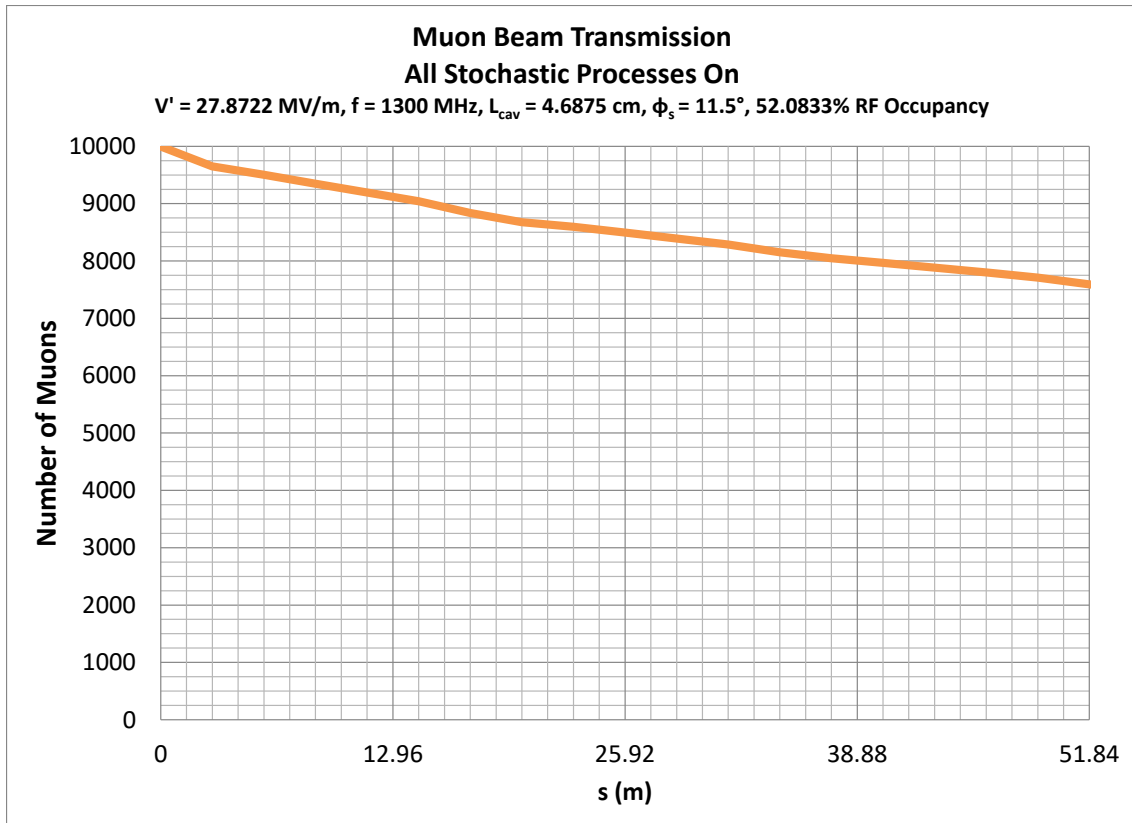

Figure 3. 76% transmission through a 51.84 meter long channel (36 full cells). At the start of the simulation there are 10000 muons. At the end of the simulation there are 7600 muons.

longer path lengths.

$$\epsilon_{x,N,\text{init}} = 0.330 \, \text{mm is formed with} \, (\sigma_x, \sigma_{p_x})_{\text{init}} = (7.785 \, \text{mm}, 4.412 \, \text{MeV/c}).$$

$$\epsilon_{y,N,\text{init}} = 0.246 \, \text{mm is formed with} \, (\sigma_y, \sigma_{p_y})_{\text{init}} = (8.147 \, \text{mm}, 3.235 \, \text{MeV/c}).$$

$$\epsilon_{L,N,\text{init}} = 0.632 \, \text{mm is formed with} \, (\sigma_z, \sigma_{p_z})_{\text{init}} = (7.4 \, \text{mm}, 8.5 \, \text{MeV/c})$$

plus an initial correlation between initial p_z and initial (radius, p_x/p_z, p_y/p_z) given by:

$$\delta p_{z_{\text{init}}} = (200 \, \text{MeV/c})((r_{\text{init}}/90.3 \, \text{mm})^2 + (p_x/p_z)^2_{\text{init}} + (p_y/p_z)^2_{\text{init}}) \tag{4.2}$$

When this correlation is added, $p_{z,\text{mean}}$ increases from 300 MeV/c to 303 MeV/c, and σ_{p_z} increases to 9.05 MeV/c. The added correlation between initial p_z and initial $(r, \, p_x/p_z, \, p_y/p_z)$ makes a small correlation between initial ϵ_{L_N} and initial $(\epsilon_{x_N}, \, \epsilon_{y_N})$. The initial (r, p_z) correlation improves initial beam matching and transmission through the lattice.

The normalized emittances decrease from

$$\epsilon_{x,y,z} = (0.330, 0.246, 0.632) \, \text{mm} \quad \text{to} \quad (0.288, 0.193, 0.618) \, \text{mm} \tag{4.3}$$

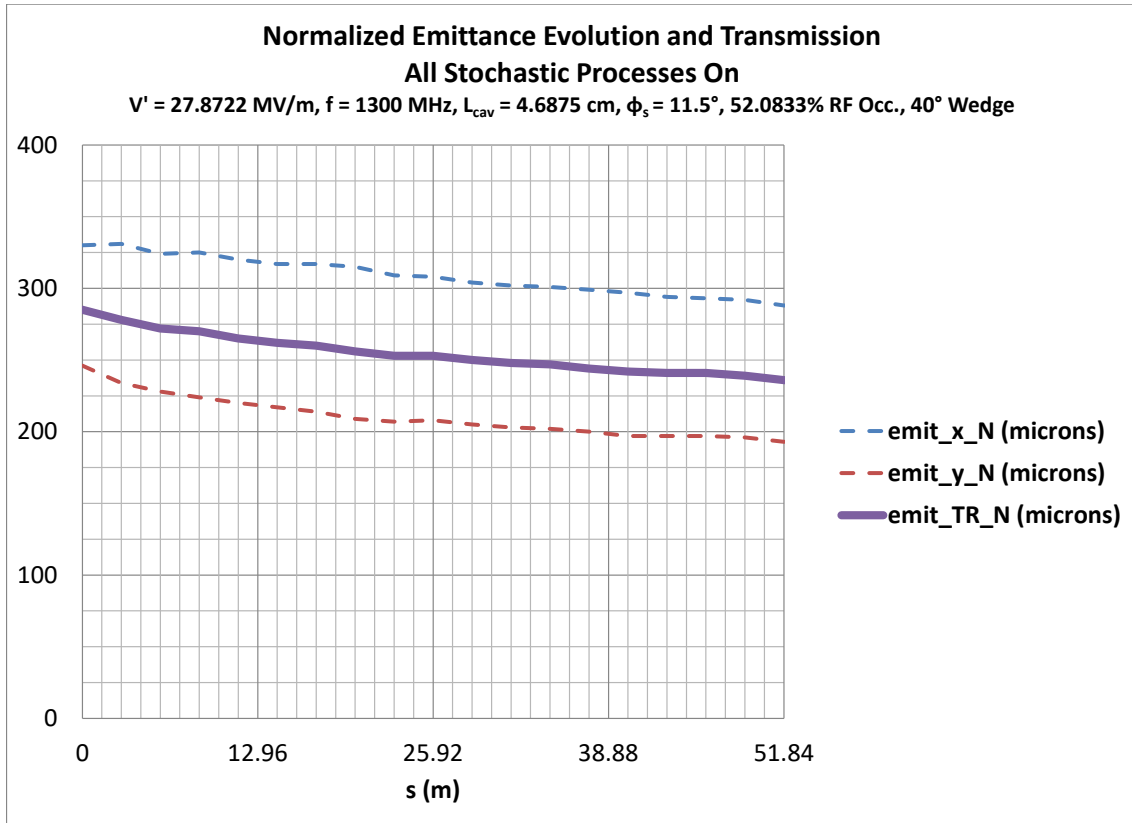as figures 4 and 5 show.There is a factor of 1.49 6D emittance reduction with 76% transmis-

Figure 4. Transverse emittance evolution for Stage 1. The total transverse emittance goes from 285 μm to 236 μm. Normalized emittance, ϵ_y, can be used with the betatron function, β_y, to calculate the size of the beam, σ_y. For example, $\sigma_y = (\beta_y \, \epsilon_y/\beta\gamma)^{1/2}$. (Emittances are measured using ICOOL's [68, 69] ecalcxy tool.)

sion through the first 36 cell stage. More stages may be possible [57]. The transmission needs improvement. The feasibility of building short, large bore quadrupoles needs to be studied.

In summary, the quadrupole channel provides a factor of 1.49 in 6D cooling in 51.84 m. For comparison the rectilinear channel [42] cools by 108,000 in 969 m and 1.84 in 51.84 m (1.84^{19} = 108,000). One might also make a comparison to the High Field – Low Momentum Final Cooling simulations [70]. This 140 m long channel has a solenoidal field of up to 30 T and a muon momentum as low as 70 MeV/c. Currently the ϵ_{xyz} normalized emittances change from (0.300, 0.300, 1.50) mm to (0.055, 0.055, 76.00) mm. Transverse to longitudinal emittance exchange works. ϵ_z is fine, but ϵ_x and ϵ_y need to be smaller for a high energy collider. The 6D emittance rises by a factor of 1.7 [(0.055 / 0.300) (0.055 / 0.300) (76.0 / 1.5)]. In the quadrupole scheme, one may be able to use wedges [27] or beam slicing [57] to decrease the final transverse emittance at the cost of the longitudinal emittance. To illustrate, the normalized longitudinal emittance that can be tolerated by a 1.5 TeV/c^2 muon collider final focus with round 750 GeV/c beams and a $\sigma_p/p = 10^{-3}$ chromaticity requirement [71] is

$$\epsilon_z = (\sigma_p/p) \Delta z (\beta\gamma) = 10^{-3} \, 10\text{mm} \, 7000 = 70 \, \text{mm} \tag{4.4}$$

where $\beta\gamma$ is the relativistic factor. A final 0.025 mm normalized transverse emittance then leads to

$$L = \frac{\gamma N^2 f_0 (DC)}{4\pi \epsilon_{x,y} \beta^*} = \frac{7000 (2 \times 10^{12})^2 \, 180,000/\text{s} \, (0.062)}{4\pi (0.0025 \, \text{cm}) \, 1.0 \, \text{cm}} = 1.0 \times 10^{34} \, \text{cm}^{-2} \, \text{s}^{-1} \tag{4.5}$$
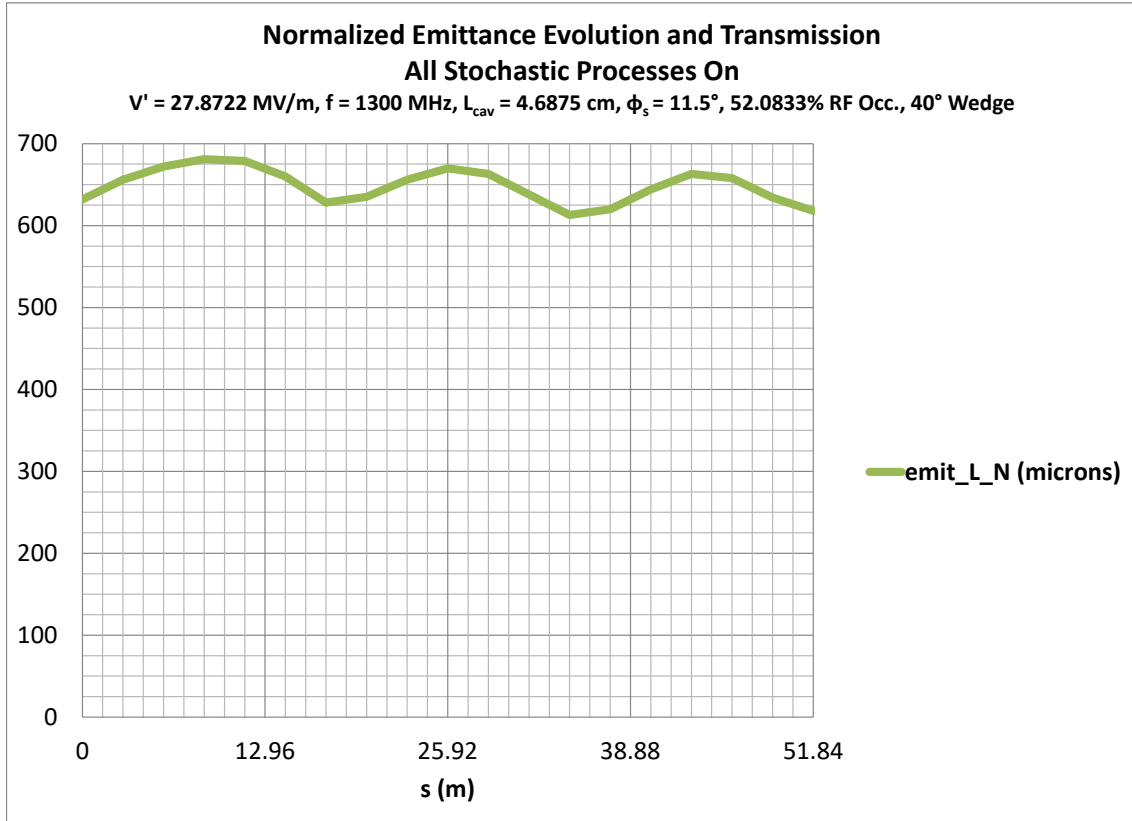

Figure 5. Longitudinal emittance evolution for Stage 1. The z-x emittance exchange prevents a natural longitudinal emittance increase. There are 36 1.44 m cells in the 51.84 m channel.

where L is average luminosity, N is the initial number of muons per bunch (one positive and one negative), f_0 is the collision frequency, DC is the duty cycle with a 15 Hz repetition rate, and β^* is the betatron function in the collision region. The beam-beam tune shift, ξ, is small enough.

$$\xi = \frac{N r_0}{4\pi\, \epsilon_{x,y}} = \frac{(2 \times 10^{12})\,(1.36 \times 10^{-14}\,\text{mm})}{4\pi\,(0.025\,\text{mm})} = 0.09 \tag{4.6}$$

Four quadrupole channels with progressively lower minimum betatron functions might be staged to achieve the sought-after factor of five in final cooling ($1.49^4 \approx 5$). Larger maximum betatron functions in these stages could be tolerated with cooler muons. Transmission in the quadrupole channel is 76%, which is too low. Ways to increase this to 90% are being sought. A final betatron function of approximately 1 cm with strong focusing quadrupoles is needed. Calculations indicate that this requirement is possible [57].

5 Parametric resonance ionization cooling

Our Muon Accelerator Program (MAP) colleagues have designed a Parametric-resonance Ionization Cooling (PIC) channel that strongly focuses a muon beam periodically [72, 73]. The beam angular spread is maximized at foci where energy absorbers are placed. The angular spread of a muon beam can be diminished until it reaches equilibrium with multiple Coulomb scattering in the absorber material. If there is more angular beam spread, there is more room to reduce the spread and cool the beam. A parametric resonance is driven by periodic quadrupoles. The quadrupole wavelength is one quarter of the wavelength of the cooling channel and drives beam oscillations. The resonance causes periodic focal points, where the beam becomes progressively narrower in x and wider in x′ as it passes down the channel. Without absorbers the beam would be unstable. Placing thin beryllium energy absorbers at the focal points stabilizes the beam by limiting the beam's angular spread at foci. Being a resonant process, focusing can be very strong without using large magnetic fields. Stronger focusing leads to cooler muons.

In the latest PIC design, skew quadrupoles are used to couple the transverse dimensions [74, 75]. Coupling may reduce the number of multipoles required for aberration correction. One may just need sextupoles and octupoles but not decapoles. Current multipole optimization controls muons up to 82 mrad. For a high luminosity, high energy muon collider, the muon beam angular spread in the PIC channel needs to be approximately 200 mrad. The angle increases if the needed output emittance is smaller (small $\beta_\perp$ required) and decreases if the available input emittance is smaller. Note that beam size and angular spreads equal $\sqrt{\beta_\perp \epsilon_\perp/(\beta\,\gamma)}$ and $\sqrt{\epsilon_\perp/(\beta_\perp\,\beta\,\gamma)}$, where $\beta_\perp$ is the transverse betatron function, $\epsilon_\perp$ is the normalized transverse beam emittance, and $\beta\,\gamma$ is the relativistic factor.

6 Passive plasma lens cooling

6.1 Observation of the focusing of electrons by a passive plasma lens

Focusing of electron beams has been predicted [76] and observed [77, 78] for passive plasma lenses. Ion beam focusing has also been studied [79].

6.2 Calculation of the focusing of muons by a passive plasma lens

A passive plasma lens is similar to a lithium lens [80] except the focusing current is in the muon beam rather than the lithium. Both follow eq. (6.1). Electrons from hydrogen or lithium hydride plasma can either be pulled in (for a μ^+ beam) or pushed out (for a μ^- beam) to cancel space charge. This leaves an azimuthal magnetic field to focus in both x and y simultaneously.

We now expand on previous work for muon cooling with plasma lenses [33, 81]. In eq. (6.1),. the track bending radius is ρ and B' is the magnetic field gradient. The longitudinal muon velocity combined with the azimuthal magnetic field produces a radial focusing force with the following equation of motion [80]:

$$\frac{d^2 r}{ds^2} + \frac{B' r}{B\rho} = 0 \tag{6.1}$$

Take a normalized longitudinal emittance [82] of 0.0006 m, 200 MeV/c muons, $\beta\gamma = p/m = 1.89$, and a momentum spread of 10%:

$$\epsilon_{LN} = \beta\gamma \, \frac{dp}{p} \, \sigma_z \qquad 2\sigma_z = \frac{2\,\epsilon_{LN}}{\beta\gamma \, \frac{dp}{p}} = \frac{2(0.0006)}{1.89\,(0.10)} = 0.0063\,\text{m} \tag{6.2}$$

A bunch length of 0.0063 m with 3×10^{12} muons [42] and $\beta = p/\sqrt{p^2 + m^2} = 0.88$ gives a beam current of

$$I = (1.6 \times 10^{-19})(3 \times 10^{12})(0.88)(3 \times 10^8 \text{m/s})/(0.0063\,\text{m}) = 20100\,\text{A} \tag{6.3}$$

The beam radius at 200 MeV/c for the end of the last stage of the rectilinear channel is:

$$\sqrt{\frac{\beta_x \, \epsilon_x}{\beta\gamma}} = \sqrt{\frac{(30.0\,\text{mm})(0.280\,\text{mm})}{1.89}} = 2.1\,\text{mm} = 0.0021\,\text{m} \tag{6.4}$$

The magnetic field at 0.0021 m with 0.68^2 of the current within 0.0021 m is:

$$B = \frac{\mu_0 \, I \, (0.68)^2}{2\pi r} = 0.89\,\text{T} \tag{6.5}$$

The field gradient, B', is 424 T/m. At p equals 0.2 GeV/c, $\beta_\perp$ is [80]

$$\beta_\perp = (B\rho/B')^{1/2} = (p/(0.3\,B'))^{1/2} = 0.040\,\text{m} = 4.0\,\text{cm} \tag{6.6}$$

Four centimeters is small enough to combine with and reduce the 3 cm betatron function in the last stage of the rectilinear channel, which should increase cooling. Note that (10^9 eV/GeV) / (3 x 10^8 m/s) = 1/0.3 and that $p = 0.3\,B\rho$. A lattice with solenoids matching into a lithium lens has been simulated [83]. As the beams gets smaller from cooling, the focusing strength increases. A small leader bunch may help to create the plasma before the main bunch arrives.

7 Conclusions

- Muons have been cooled using ionization at MICE.

- Cooling by about a factor of 100, 000 has been achieved in simulation. Another cooling factor of five is needed to reach a luminosity of 10^{34} cm^{-2} s^{-1} for a high energy muon collider.

- The peak RF power needed by the rectilinear cooling channel is 72% of the RF previously installed at SLAC. Muons of each sign may be able to travel in opposite directions though each of the 12 stages of the rectilinear channel, before proceeding to the next stage. Thus, only one channel would be needed for both signs.

- Hydrogen gas has been experimentally used to prevent RF breakdown in the presence of ionizing beams and magnetic fields. The hydrogen may also neutralize space charge permitting shorter bunches and more longitudinal cooling and possibly allowing the magnetic field from the beam current to focus the beam itself for more transverse cooling. Short bunches increase instantaneous beam current.

- Reducing momentum compaction has been shown to decrease longitudinal emittance in the simulation of the latest helical cooling channel [33] by a factor of 1.7 to 0.890 mm.

- Stronger focusing can transversely cool muons beyond the reach of solenoidal channels for a given magnetic field. 6D cooling by a factor of 1.49 in a 51.84 m long strong focusing quadrupole channel is observed in simulation. A y emittance of 0.193 mm is achieved, lower than in the helical and rectilinear channels.

- If a cooling combination can reach $\epsilon_{x,y,z}$(0.190, 0.190, 0.700) mm $\rightarrow$ 0.025 mm^3 with adequate transmission, cooling is complete for a 10^{34} cm^{-2} s^{-1} luminosity, high energy muon collider. The idea is to lower longitudinal emittance with reduced momentum compaction plus higher RF frequency and then to add a final low beta stage for more transverse cooling.

References

[1] Y. Alexahin et al., *The Case for a Muon Collider Higgs Factory*, in *Proceedings, 2013 Community Summer Study on the Future of U.S. Particle Physics: Snowmass on the Mississippi (CSS2013): Minneapolis, MN, U.S.A., July 29 – August 6, 2013*, [arXiv:1307.6129].

[2] Y. Alexahin et al., *Muon Collider Higgs Factory for Snowmass 2013*, in *Proceedings, 2013 Community Summer Study on the Future of U.S. Particle Physics: Snowmass on the Mississippi (CSS2013): Minneapolis, MN, U.S.A., July 29 – August 6, 2013*, [arXiv:1308.2143].

[3] C. Rubbia, *Further searches of the Higgs scalar sector at the ESS*, arXiv:1908.05664.

[4] D.V. Neuffer and R.B. Palmer, *A High-Energy High-Luminosity $\mu^+ - \mu^-$ Collider*, *Conf. Proc.* **C 940627** (1995) 52.

[5] C.M. Ankenbrandt et al., *Status of muon collider research and development and future plans*, *Phys. Rev. ST Accel. Beams* **2** (1999) 081001 [`physics/9901022`].

[6] R.B. Palmer, *Muon Colliders*, *Rev. Accel. Sci. Tech.* **7** (2014) 137.

[7] D.J. Summers, L.M. Cremaldi, R. Godang, B.R. Kipapa, H.E. Rice and R.B. Palmer, *Muon acceleration to 750 GeV in the Tevatron tunnel for a 1.5 TeV $\mu^+\mu^-$ collider*, *Conf. Proc.* **C 070625** (2007) 3178 [`arXiv:0707.0302`].

[8] C. Albright et al., *Physics at a neutrino factory*, `hep-ex/0008064`.

[9] IDS-NF collaboration, *International Design Study for the Neutrino Factory, Interim Design Report*, `arXiv:1112.2853`.

[10] D. Neuffer, *Comments on Ionization Cooling Channel Characteristics*, 2017 *JINST* **12** T09004 [`arXiv:1312.1266`].

[11] D. Neuffer, *Principles and Applications of Muon Cooling*, *Part. Accel.* **14** (1983) 75.

[12] MICE collaboration, *The MICE Muon Beam on ISIS and the beam-line instrumentation of the Muon Ionization Cooling Experiment*, 2012 *JINST* **7** P05009 [`arXiv:1203.4089`].

[13] MICE collaboration, *Lattice design and expected performance of the Muon Ionization Cooling Experiment demonstration of ionization cooling*, *Phys. Rev. Accel. Beams* **20** (2017) 063501 [`arXiv:1701.06403`].

[14] MICE collaboration, *First particle-by-particle measurement of emittance in the Muon Ionization Cooling Experiment*, *Eur. Phys. J.* **C 79** (2019) 257 [`arXiv:1810.13224`].

[15] D.M. Kaplan, K. Long and J. Nugent, *Progress in Muon Ionization Cooling Demonstration with MICE*, COOL-2019-TUY02.

[16] MICE collaboration, *First Demonstration of Ionization Cooling in MICE*, in *Proceedings, 9th International Particle Accelerator Conference (IPAC 2018): Vancouver, BC Canada, April 29 – May 4, 2018*, p. FRXGBE3, 2018, DOI [`arXiv:1806.01807`].

[17] V. Bayliss et al., *The Liquid-Hydrogen Absorber for MICE*, *IOP Conf. Ser. Mater. Sci. Eng.* **502** (2019) 012150.

[18] MICE collaboration, *The liquid-hydrogen absorber for MICE*, 2018 *JINST* **13** T09008 [`arXiv:1807.03019`].

[19] D. Rajaram and V. Blackmore, *Phase Space Density Evolution in MICE*, in *Proceedings, 9th International Particle Accelerator Conference (IPAC 2018): Vancouver, BC Canada, April 29 – May 4, 2018*, p. TUPML065, [`arXiv:1806.04299`].

[20] MICE collaboration, *A Non-parameteric Density Estimation Approach to Measuring Beam Cooling in MICE*, in *Proceedings, 9th International Particle Accelerator Conference (IPAC 2018): Vancouver, BC Canada, April 29 – May 4, 2018*, p. TUPML063, 2018, DOI [`arXiv:1806.01834`].

[21] F. Drielsma, *Measurement of the increase in phase space density of a muon beam through ionization cooling*, GENEVA-THESE-5249 (2018).

[22] MICE collaboration, *Recent results from MICE on multiple Coulomb scattering and energy loss*, in *Proceedings, 9th International Particle Accelerator Conference (IPAC 2018): Vancouver, BC Canada, April 29 – May 4, 2018*, p. THPML058, [`arXiv:1805.07128`].

[23] D. Attwood et al., *The scattering of muons in low Z materials*, *Nucl. Instrum. Meth.* **B 251** (2006) 41 [`hep-ex/0512005`].

[24] MICE collaboration, *A Wedge Test in MICE*, in *Proceedings, 9th International Particle Accelerator Conference (IPAC 2018): Vancouver, BC Canada, April 29 – May 4, 2018*, p. TUPML062, [`arXiv:1806.01824`].

[25] T.A. Mohayai, *A Novel Non-Parametric Density Estimation Approach to Measuring Muon Ionization Cooling and Reverse Emittance Exchange in the MICE Experiment*, FERMILAB-THESIS-2018-31 (2018).

[26] C. Brown and C. Whyte, *Emittance Exchange in MICE*, IPAC-2019-WEPTS108.

[27] D. Neuffer, *Phase Space Exchange in Thick Wedge Absorbers for Ionization Cooling*, *AIP Conf. Proc.* **441** (1998) 270.

[28] MICE collaboration, *Pion Contamination in the MICE Muon Beam*, 2016 *JINST* **11** P03001 [`arXiv:1511.00556`].

[29] MICE collaboration, *The design and commissioning of the MICE upstream time-of-flight system*, *Nucl. Instrum. Meth.* **A 615** (2010) 14 [`arXiv:1001.4426`].

[30] L. Cremaldi, D.A. Sanders, P. Sonnek, D.J. Summers and J. Reidy Jr., *A Cherenkov Radiation Detector with High Density Aerogels*, *IEEE Trans. Nucl. Sci.* **56** (2009) 1475 [`arXiv:0905.3411`].

[31] MICE collaboration, *Demonstration of cooling by the Muon Ionization Cooling Experiment*, *Nature* **578** (2020) 53 [`arXiv:1907.08562`].

[32] C. Yoshikawa et al., *Status of the Complete Muon Cooling Channel Design and Simulations*, IPAC-2014-TUPME016.

[33] K. Yonehara, *Helical Six-Dimensional Muon Ionization Cooling Channel with Gas-Filled RF Cavities*, 2018 *JINST* **13** P09003 [`arXiv:1806.00129`].

[34] W.H. Bennett, *Magnetically Self-Focussing Streams*, *Phys. Rev.* **45** (1934) 890.

[35] W.E. Parkins, *The Uranium Bomb, the Calutron, and the Space-Charge Problem*, *Phys. Today* **58N5** (2005) 45.

[36] D. Stratakis, R.B. Palmer and D.P. Grote, *Influence of space-charge fields on the cooling process of muon beams*, *Phys. Rev. ST Accel. Beams* **18** (2015) 044201.

[37] NEUTRINO FACTORY AND MUON COLLIDER collaboration, *The effects of surface damage on RF cavity operation*, *Phys. Rev. ST Accel. Beams* **9** (2006) 062001.

[38] D. Stratakis, J.C. Gallardo and R.B. Palmer, *Effects of external magnetic fields on the operation of high-gradient accelerating structures*, *Nucl. Instrum. Meth.* **A 620** (2010) 147.

[39] M. Chung et al., *Pressurized* $\mathbf{H_2}$ *RF Cavities in Ionizing Beams and Magnetic Fields*, *Phys. Rev. Lett.* **111** (2013) 184802.

[40] P. Snopok and J. Ellison, *Progress on Beam-Plasma Effect Simulations in Muon Ionization Cooling Lattices*, in *Proceedings, 9th International Particle Accelerator Conference (IPAC 2018): Vancouver, BC Canada, April 29 – May 4, 2018*, p. TUPML066, [`arXiv:1806.04203`].

[41] D. Bowring et al., *Operation of normal-conducting RF cavities in multi-tesla magnetic fields for muon ionization cooling: a feasibility demonstration*, [`arXiv:1807.03473`].

[42] D. Stratakis and R.B. Palmer, *Rectilinear six-dimensional ionization cooling channel for a muon collider: A theoretical and numerical study*, *Phys. Rev. ST Accel. Beams* **18** (2015) 031003.

[43] V. Balbekov, *R_FOFO snake channel for 6D muon cooling ("R" can be interpreted as "Rectilinear")*, MAP-DOC-4365 (2013).

[44] Matthew Sands, *The Physics of Electron Storage Rings: An Introduction*, SLAC-R-121 (1970) eq. 2.128.

[45] D. Stratakis, R.C. Fernow, J.S. Berg and R.B. Palmer, *Tapered channel for six-dimensional muon cooling towards micron-scale emittances*, *Phys. Rev. ST Accel. Beams* **16** (2013) 091001.

[46] D. Stratakis, *A hybrid six-dimensional muon cooling channel using gas filled rf cavities*, 2017 *JINST* **12** P09027 [arXiv:1709.02331].

[47] J.C. Gallardo et al., *$\mu^+\mu^-$ Collider: Feasibility Study*, Snowmass 1996, SLAC-R-988.

[48] Y. Bao, G. Hanson, R.B. Palmer and D. Stratakis, *Conceptual design and modeling of a six-dimensional bunch merging scheme for a muon collider*, *Phys. Rev. Accel. Beams* **19** (2016) 031001.

[49] R.B. Palmer et al., *A Complete Scheme of Ionization Cooling for a Muon Collider*, *Conf. Proc.* **C 070625** (2007) 3193 [arXiv:0711.4275].

[50] R.B. Palmer et al., *An Induction Kicker for Muon Cooling Rings*, NFMCC-DOC-256 (2002).

[51] D. Li, private communication.

[52] R.P. Borghi, *Design and Fabrication of the Accelerating Structure for the Stanford 2-Mile Accelerator*, SLAC-PUB-0071 (1965).

[53] M. Ross, private communication.

[54] K. Hubner, *The LEP Superconducting RF System*, SNOWMASS-2001-M304.

[55] R. Cliff et al., *Developments and directions in 200 MHz very high power RF at LAMPF*, LA-UR-91-3102 (1991).

[56] S. Feher and J. Strait, *Estimated Inner Triplet Quadrupole Length and Aperture for Really Large Hadron Colliders of $E_{\text{beam}} = 30$, 60 and 100 TeV*, Snowmass-1996-ACC042.

[57] D.J. Summers et al., *Final Muon Emittance Exchange in Vacuum for a Collider*, IPAC-2015-TUPWI044 (2015).

[58] J.G. Acosta, *Final Cooling for a Muon Collider*, FERMILAB-THESIS-2017-15 (2017).

[59] C. Johnstone, M. Berz, D. Errede and K. Makino, *Muon beam ionization cooling in a linear quadrupole channel*, *Nucl. Instrum. Meth.* **A 519** (2004) 472.

[60] R. Baartman, *Quadrupole shapes*, *Phys. Rev. ST Accel. Beams* **15** (2012) 074002.

[61] Al Garren and Harold Kirk, *Muon Cooling Ring Lattices with Quadrupoles and Dipoles*, MAP-DOC-4408 (2002).

[62] H. Kirk, D. Cline, Y. Fukui and A. Garren, *Muon storage rings for 6D phase-space cooling*, *Conf. Proc.* **C 030512** (2003) 2008.

[63] A. Garren, D. Cline, S. Kahn, H. Kirk and F.E. Mills, *6-D cooling of a circulating muon beam*, *AIP Conf. Proc.* **821** (2006) 415.

[64] Neutrino Factory and Muon Collider collaboration, *Recent Progress in Neutrino Factory and Muon Collider Research within the Muon Collaboration*, *Phys. Rev. ST Accel. Beams* **6** (2003) 081001 [hep-ex/0207031].

[65] H. Grote et al., *MAD-X Methodical Accelerator Design Version 5.02.08 User's Reference Manual*, (2016).

[66] W. Herr and F. Schmidt, *A MAD-X Primer*, CERN-AB-2004-027-ABP.

[67] E.D. Courant and H.S. Snyder, *Theory of the alternating gradient synchrotron*, *Annals Phys.* **3** (1958) 1.

[68] R.C. Fernow, *ICOOL: A simulation code for ionization cooling of muon beams*, *eConf* **C990329** (1999) THP31.

[69] R.C. Fernow, *Recent developments on the muon-facility design code ICOOL*, *Conf. Proc.* **C 0505161** (2005) 2651.

[70] Hisham Kamal Sayed, Robert B. Palmer and David Neuffer, *High Field-Low Energy Muon Ionization Cooling Channel*, *Phys. Rev. ST Accel. Beams* **18** (2015) 0919001.

[71] Neutrino Factory and Muon Collider collaboration, *Muon Collider Interaction Region Design*, *Conf. Proc.* **C 100523** (2010) TUPEB022 [arXiv:1202.0198].

[72] Ya.S. Derbenev et al., *Parametric-resonance Ionization Cooling of Muon Beams*, arXiv:1205.3476.

[73] V.S. Morozov, Ya.S. Derbenev, A. Afanasev, R.P. Johnson, B. Erdelyi and J.A. Maloney, *Parametric-resonance ionization cooling of muon beams*, *AIP Conf. Proc.* **1507** (2012) 843.

[74] A. Afanasev et al., *Skew-Quad Parametric-Resonance Ionization Cooling: Theory and Modeling*, IPAC-2015-TUPHA013.

[75] A. Sy et al., *Aberration Compensation in a Skew Parametric-Resonance Ionization Cooling Channel*, IPAC-2017-WEPIK116.

[76] J.B. Rosenzweig and P. Chen, *Beam Optics of a Selffocusing Plasma Lens*, *Phys. Rev.* **D 39** (1989) 2039.

[77] H. Nakanishi et al., *Direct observation of plasma lens effect*, *Phys. Rev. Lett.* **66** (1991) 1870.

[78] G. Hairapetian et al., *Experimental demonstration of dynamic focusing of a relativistic electron bunch by an overdense plasma lens*, *Phys. Rev. Lett.* **72** (1994) 2403.

[79] A. Yuen, S.M. Lund, J.J. Barnard, R.H. Cohen and J.S. Wurtele, *Scattering effects in passive foil focusing of ion beams*, *Phys. Rev. ST Accel. Beams* **18** (2015) 091301.

[80] A. Hassanein et al., *The design of a liquid lithium lens for a muon collider*, *Conf. Proc.* **C 990329** (1999) 3062.

[81] R. Palmer, D.V. Neuffer and J.C. Gallardo, *A practical high-energy high-luminosity $\mu^+ - \mu^-$ collider*, *AIP Conf. Proc.* **335** (1995) 635.

[82] R.B. Palmer, *Muon Colliders*, BNL-90950-2010-CP.

[83] Y. Fukui, D.B. Cline, A.A. Garren and H.G. Kirk, *Progress in designing a muon cooling ring with lithium lenses*, PAC-2003-TPPB084.